# Simultaneous production of cooling and freshwater by an integrated indirect evaporative cooling and humidification-dehumidification desalination cycle

Qian Chen[1,*], Muhammad Burhan[1], Muhammad Wakil Shahzad[1,2], Doskhan Ybyraiymkul[1], Faheem Hassan Akhtar[1], Kim Choon Ng[1,*]

1. *Water Desalination and Reuse Center, King Abdullah University of Science and Technology, Thuwal 23955, Saudi Arabia*
2. *Northumbria University, Newcastle upon Tyne, United Kingdom*

*Corresponding Authors, email: chen_qian@u.nus.edu; kimchoon.ng@kaust.edu.sa

## Abstract

Cooling and freshwater represent two fundamental demands in hot and arid regions. This paper reports the integration of an indirect evaporative cooler (IEC) and a humidification-dehumidification desalination cycle (HDH) for the simultaneous production of cooling and freshwater. To take full advantage of system integration, the purge air from IEC is supplied to HDH to promote water productivity. A pilot IEC unit is firstly designed and tested to achieve the temperatures and humidity of the outlet air steams. Results reveal that the IEC unit is able to cool down the supply air to below 25 ℃ under different outdoor conditions, and the purge air temperature is also 5-10 ℃ lower than the intake air temperature. Employing the IEC purge air as the working air, the HDH cycle is then investigated analytically. Under the operation ranges considered, the freshwater productivity and gain-output ratio (GOR) are 25-125 L/hr and 1.6-2.5, respectively, which are higher than other HDH configurations operating under the same conditions. Finally, the performance of the combined IEC-HDH system is evaluated. The overall coefficient of performance (COP) and Second-law efficiency are found to be 2.1-2.5 and 3-26%, respectively. Further improvement of efficiency can be achieved by integrating with adsorption or vapor compression refrigeration cycles.

*Keywords:* indirect evaporative cooling; humidification dehumidification desalination; system integration; cooling/freshwater cogeneration; experimental study;

## 1. Introduction

Cooling and freshwater are two basic demands in hot and arid regions. In the Gulf Cooperation Council (GCC) countries, annual water consumption has exceeded 26 billion $m^3$ [1], while the cooling demand is more than 36 million Rton [2]. The demands will further expand due to rapid population growth as well as the increase of living standards.

Desalination provides a reliable solution to the issues associated with water scarcity. So far, nearly 20,000 desalination plants have been installed, and global desalination capacity exceeds 100 million $m^3$/day [3]. Around 57% of the desalination capacity is located in GCC countries, accounting for >50% of the global desalination output [1]. Consequently, due to the energy-intensive nature of the existing desalination technologies, e.g. reverse osmosis (RO), multi-effect distillation (MED), and multi-stage flash distillation (MSF), a significant portion of natural energy resources (oil and gas) produced in these countries are consumed for desalination [4]. With the depletion of fossil fuels, the exploration of novel desalination processes driven by renewable energy sources has attracted interests at both research and industrial levels. Among all the emerging desalination technologies, humidification-dehumidification desalination (HDH) has gained much attention due to several promising features. It has a low operation temperature (50-70 ℃),

simple system components, easy maintenance and operation, and low initial plant costs. These advantages distinguish HDH from other desalination processes, making it suitable for integration with renewable energy sources [5].

The demand for cooling is provided by electricity-driven mechanical chillers. In GCC countries, the energy consumption for cooling is over 3 times as compared to that of other regions due to the severe weather conditions, and cooling systems consume 50-70% of peak electricity [2]. To reduce fossil fuel consumption, indirect evaporative cooling (IEC) has been considered to replace mechanical chillers. IEC utilizes the evaporative potential of unsaturated air for cooling purposes, and only minor electricity is consumed to power the fans and the water pumps. Among different IEC configurations, the regenerative IEC, which is initiated by the Maisotsenko cycle (M-cycle), shows the greatest potential [6]. In an M-cycle, the working air is pre-cooled in the dry channels before being directed into the wet channels, thus allowing the supply air to be cooled to below the web bulb temperature and approach the dew point temperature.

Both HDH and IEC have attracted a lot of attention in recent years. HDH has been integrated with various systems to meet different demands and improve energy efficiency. Qasem and Zubair [7] proposed an air-heated HDH system integrated with an adsorption (AD) desalination system. The gain-output-ratio (GOR) of the hybrid system was found to be higher than the conventional HDH system. Chiranjeevi and Srinivas [8] integrated a two-stage HDH system with a single-effect absorption refrigeration (VAR) plant, which was able to simultaneously produce freshwater and cooling effects at 670 LPH and 75 kW, respectively. Sadeghi et al. [9] reported a multi-generation hybrid system combining a water-heated HDH cycle, an organic Rankine cycle, and an ejector refrigeration cycle. The combined system achieved an overall exergy efficiency of 17.12%. He et al. [10, 11] coupled a mechanical compression heat pump with a water-heated HDH system. The freshwater productivity was observed to be 82 LPH, and the GOR was 5.14. Xu, Sun, and Dai [12] also combined HDH with a heat pump, but they employed moist air as the working fluid of the heat pump. Under a spraying water temperature of 70 ℃, the system achieved a specific energy consumption of 18.35 kg/kWh.

Studies on improving the IEC cycle have also been extensively reported. Sayyaadi and Hoseinpoori [13] conducted a multi-objective optimization of a cross-flow indirect evaporative cooler using the data handling-type neural network. COP and energy efficiency were improved by 8.1% and 6.9%, respectively, after optimization. Sohani, Sayyaadi, and Zeraatpisheh [14] used an hourly optimization strategy to optimize the annual performance of IEC. Energy efficiency, water consumption, and economic index were increased by 17.8%, 19.6%, and 36.2%, respectively. Akhaghi et al. [15] optimized a counter-flow dew-point cooler using the Genetic Algorithm. Up to 72% of improvement in COP was achieved. Cui et al. [16] employed a desiccant dehumidifier to dehumidify the intake air before supplying it to IEC. Due to the pre-dehumidification effect, the temperature of the product air could be reduced to below the dew-point temperature of the intake air. Woods and Kozubal [17] presented a detailed model for a combined liquid desiccant and evaporative cooling system. The model prediction agreed with the experimental results within 10% discrepancies. Pandelidis et al. [18] compared different evaporative coolers combined with desiccant wheels. The system with the cross-flow M-Cycle unit obtained the lowest supply air temperatures and largest cooling capacities. Cui [19, 20] et al. combined IEC with a vapor compression system. IEC was able to fulfill 47% of the cooling load while significantly reducing electricity consumption. Tariq et al. [21] reversed the IEC to work as an air saturator of a desalination system, and the performance was observed to be better than conventional desalination plants. Sahafifar and Gadalla [22] used the M-cycle as the air saturator of a gas turbine, which improved the shaft power output and efficiency.

In light of the promising features of IEC and HDH, it is natural to consider the combination of them for the simultaneous production of freshwater and cooling effects in hot and arid areas. Comparing to other

combined systems for cogeneration of cooling and freshwater (e.g. adsorption cooling/desalination system [23], HDH integrated with the absorption cycle [8], HDH combined with vapor compression refrigeration cycle [10, 11]), the IEC-HDH cycle has many advantages. Firstly, both IEC and HDH have are made up of simple components, thus eliminating the need for complicated equipment like adsorption beds and compressors. Secondly, the IEC-HDH cycle works under the ambient condition, and there is little requirement for maintenance and operation. Thirdly, the primary energy consumption of the system is small, since IEC is energy-efficient, while HDH employs low-grade heat as the energy source. In addition, since both systems use air as one of the working media, the purge air from the IEC, which has a lower temperature than the ambient, can be supplied to the HDH to further promote productivity and energy efficiency. Due to these promising features, the proposed IEC-HDH cycle will be economically competitive and environmentally friendly.

An experimental investigation of the integrated IEC-HDH cycle has been reported by Kabeel, Abdelgaied, and Feddaoui [24]. Under the climatic conditions of Tanta city, Egypt, the cooling load of the system ranged from 253 to 417 W, and the daily water productivity varied from 35 to 47 L. The system demonstrated the great potential of the integrated IEC-HDH cycle for cooling and desalination applications in remote areas. However, there are several limitations with their study. Firstly, the derived results are based on dynamic climatic conditions (varying heat source and ambient temperatures), and the impacts of each variable on system performance were not well analyzed. To enable a better understanding of the system, it is crucial to conduct a parametric study on each design and operating variable. Secondly, only the performance of the integrated system was reported, while the benefit of system integration was not well demonstrated. Therefore, whether the combined system outperforms the standalone IEC and HDH systems remains questionable. Thirdly, the study is based on energy analysis. An exergy analysis will provide thermodynamic insights on the system irreversibility and internal dissipations, but exergy performance on the integrated IEC-HDH cycle was not covered. Finally, a comparison with other similar systems will help to highlight the merits of the proposed IEC-HDH cycle and identify the potential for further improvement, yet such information is not provided. Except for the aforementioned study, thus far, no other study is available in the literature that investigates an integrated IEC-HDH system.

This paper is intended to conduct a systematic study on the integrated IEC-HDH cycle to cover the afore-mentioned research gaps. A pilot IEC unit will be designed and tested first to obtain the temperatures and humidity for purge air and supply air under different intake air temperatures. Then the productivity and energy efficiency of the HDH cycle will be evaluated employing the IEC purge air as the working air. The performance of other HDH cycles under the same conditions will also be presented to highlight the advantages of system integration. Finally, the overall energy and exergy efficiency of the integrated IEC-HDH cycle will be calculated and compared with similar systems.

## 2. Process description

Figure 1 shows the working principle of the integrated indirect evaporative cooling-humidification dehumidification desalination (IEC-HDH) cycle, which consists of an IEC unit and an HDH system. The IEC is made up of alternating dry and wet channels, and the HDH unit includes a humidifier, a dehumidifier, and a water heater. Outdoor air (1/1') is firstly supplied to the dry channels of the IEC to be cooled. Then a portion of the air (2, supply air) is supplied to the buildings, while the remaining (3, purge air) enters the wet channels. The wet channels are sprayed with water (either in the form of droplets or films), and evaporation is induced due to the partial vapor pressure difference between water and air. The latent heat of vaporization lowers the temperature of the water film and the channel walls, which then cool down the air in the dry channels. The purge air, which is disposed of in a regular IEC unit, is used as the working air

in the HDH cycle. It firstly enters the humidifier to get heated and humidified by the hot seawater (process 3-4). Then it is directed to the dehumidifier, where it is cooled down by the feed seawater (stream 6) and the moisture content is condensed (4-5). The distillate (stream 10) is collected as the product water, while the preheated seawater is further heated using external heat sources (stream 11) before being sprayed into the humidifier.

Figure 2 shows the process of the proposed IEC-HDH cycle in the psychrometric chart. The numbers for the state points are adopted from Figure 1. Process 1-2-3 represents the IEC cycle, and 3-4-5 is the HDH cycle. A basic HDH cycle (1'-4'-5') is also presented in the chart for comparison. In the integrated IEC-HDH cycle, the working air enters the humidifier at a lower temperature. Therefore, it is expected to promote evaporation due to a larger driving force, which will improve water productivity and energy efficiency.

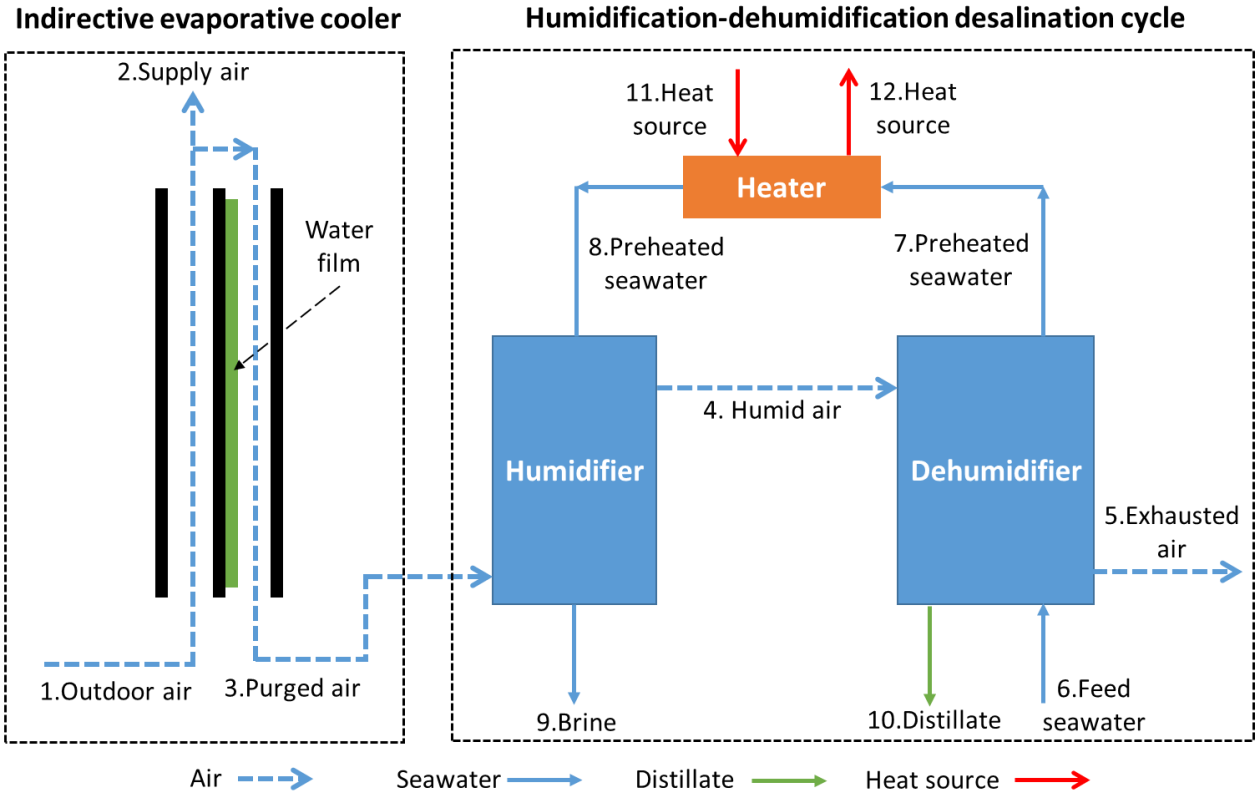


Figure 1 Schematic of the integrated indirect evaporative cooling-humidification dehumidification cycle

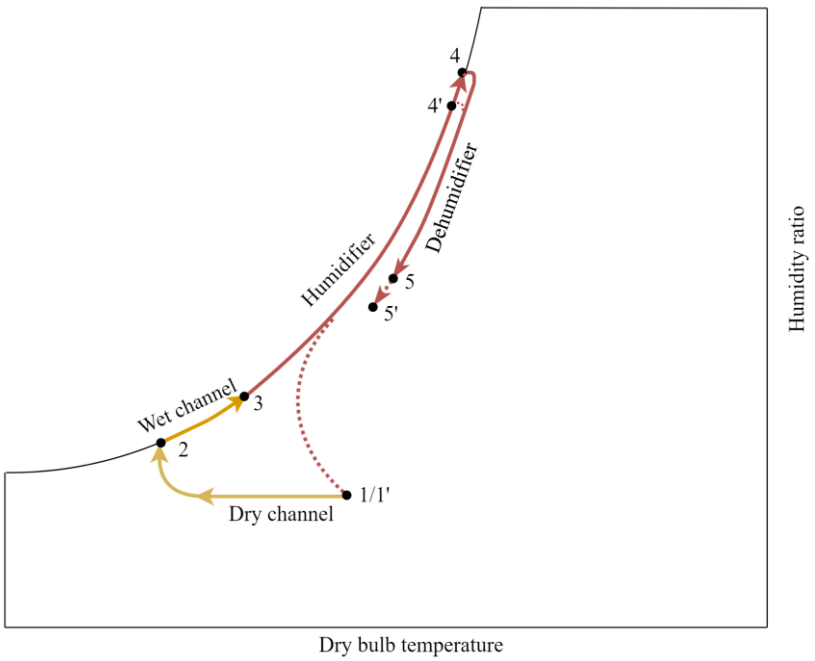


Figure 2 Path of the air in the psychrometric chart for the proposed IEC-HDH cycle (1-2-3-4-5) and a basic HDH cycle (1'-4'-5'). The numbers for state points are adopted from Figure 1

## 3. Experimental setup

A pilot IEC unit has been developed in Water Desalination and Reuse Center, King Abdullah University of Science and Technology (KAUST). Figure 3(a) shows a schematic of the pilot unit, consisting of a heat and mass exchanger, a spray pump, a set of water nozzles, a centrifugal fan, a control box, as well as air ducts, dampers, and supporting frames. The centrifugal fan is located at the exit of the dry channels, while the spray nozzles are installed on the top of the wet channels.

The heat and mass exchanger is the key component of the IEC unit. It consists of 50 air channels (25 dry channels and 25 wet channels). The channel walls are made of aluminum foils with a thickness of 300 μm, and acrylic spacers are placed between the walls for supporting purposes. Each foil has a dimension of 1 m × 1 m with 200 mm × 300 mm chamfers at the four corners. Figure 3(b) is a photo of the heat and mass exchanger.

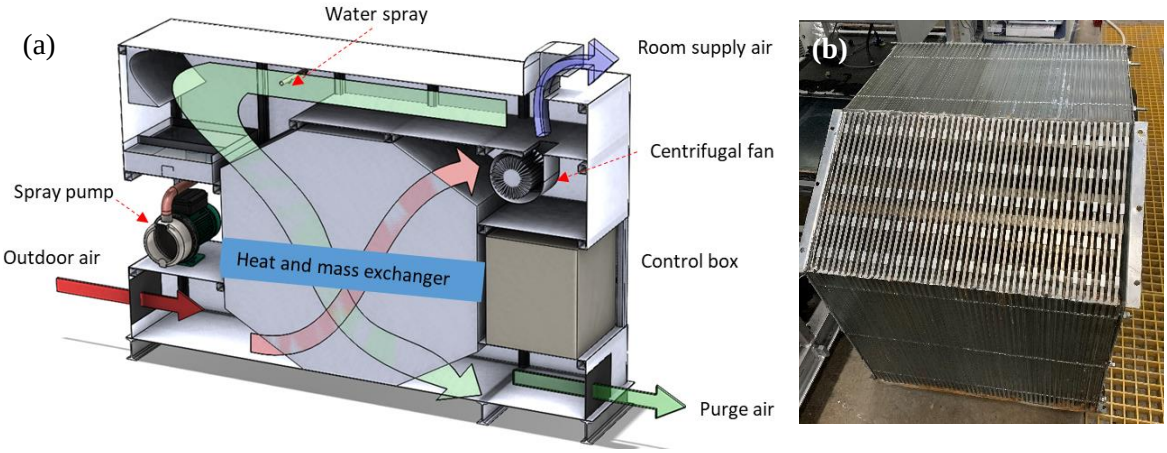


Figure 3 (a) Schematic of the IEC unit, and (b) heat and mass exchanger

To monitor the performance of the IEC unit, sensors are installed at the inlets and outlets of the dry and wet channels to measure the temperature, humidity, and velocity of the air streams. Temperatures are measured using thermistor probes (TJ36-44004-1/8-12, OMIGA [25]), while both humidity and velocity are measured using the air humidity/velocity probes (FH400, Degree Controls Inc. [26]). The thermistor probes were calibrated using a master mercury thermometer with an accuracy of ± 0.1 °C, while calibration data provided by the manufacturer were employed for the air humidity/velocity probes. Table 1 summarizes the measurement uncertainties of these sensors. The signal outputs of these sensors are recorded using a data logger (Agilent 34970A) in 10-s intervals for further analysis.

Table 1 Measurement uncertainties for different parameters

| Parameter | Range | Nominal value[a] | Absolute uncertainty | Relative uncertainty[b] |
|---|---|---|---|---|
| Air temperature | 22-42 °C | 32 °C | ± 0.1 °C [25] | 0.31% |
| Relative humidity | 10-100% | 50% | ± 2% [26] | 4% |
| Air velocity | 1-3 m/s | 2 m/s | ± 0.1 m/s [26] | 5% |

a. The average value of the parameters;
b. Absolute uncertainty divided by the nominal value;

## 4. Mathematical modelling

The performance of the HDH cycle and the integrated IEC-HDH cycle is evaluated via thermodynamic analysis. Governing equations for the HDH cycle are firstly derived to obtain the states of different streams in different locations. Then productivity and energy efficiency of the HDH cycle and the integrated system can be obtained.

### 4.1 HDH cycle

Considering steady-state operation without heat loss to the ambient, the performance of the HDH cycle can be predicted by analyzing heat and mass balances in different system components. Referring to the state points shown in Figure 1, the governing equations are summarized in Table 2.

Other key assumptions and simplifications for the HDH cycles include:

(1) The effectiveness of both the humidifier and the dehumidifier is considered to be 0.8, while the effectiveness of the heater is assumed to be 0.7 [9];

(2) The moist air leaves the humidifier and the dehumidifier with a relative humidity of 100% [27];

(3) The properties of air and water are assumed to be uniform in each component, and they are calculated according to the average temperature, moisture content, and salinity. Seawater properties are calculated using correlations developed by Sharqawy and Lienhard [28], and moist air properties are obtained using equations developed by Herrmann, Kretzschmar, and Gatley [29].

Table 2 Mathematical model for the HDH cycle

| Component | Equation | No. | Comment |
|---|---|---|---|
| **Humidifier** | $\dot{m}_{w8} - \dot{m}_{w9} = \dot{m}_{da}(\omega_4 - \omega_3)$ | (1) | Humidifier mass balance; |
| | $\dot{m}_{w8}h_{w8} - \dot{m}_{w9}h_{w9} = \dot{m}_{da}(h_{a4} - h_{a3})$ | (2) | Humidifier energy balance; |
| | $\varepsilon_{hum} = \max\{\frac{h_{w8}-h_{w9}}{h_{w8}-h_{w9,ideal}}, \frac{h_{a4}-h_{a3}}{h_{a4,ideal}-h_{a3}}\}$ | (3) | Humidifier effectiveness; |
| **Dehumidifier** | $\dot{m}_{w10} = \dot{m}_{da}(\omega_4 - \omega_5)$ | (4) | Dehumidifier mass balance; |
| | $\dot{m}_{da}(h_{a4} - h_{a5}) - \dot{m}_{w10}h_{w10} = \dot{m}_{w6}(h_{w7} - h_{w6})$ | (5) | Dehumidifier energy balance; |
| | $\varepsilon_{deh} = \max\{\frac{h_{w7}-h_{w6}}{h_{w7,ideal}-h_{w6}}, \frac{h_{a4}-h_{a5}}{h_{a4}-h_{a5,ideal}}\}$ | (6) | Dehumidifier effectiveness; |
| **Heater** | $\varepsilon_{hex}\Delta H_{max} = \dot{m}_{w7}(h_{w8} - h_{w7})$ | (7) | Heater energy balance; |
| | $\Delta H_{max} = C_{min}(T_{w11} - T_{w7})$ | (8) | Maximum possible heat transfer; |
| | $C_{min} = \min\{\dot{m}_{w7}c_{pw}, \dot{m}_{w11}c_{pw}\}$ | (9) | Minimum thermal mass; |
| **System performance** | $GOR = \frac{\dot{m}_{w10}h_{fg}}{\dot{m}_{w11}(h_{w11} - h_{w12})}$ | (10) | Gain-output-ratio; |

### 4.2 Integrated IEC-HDH cycle

The performance of the integrated cycle can be measured by the overall energy efficiency, which is expressed as the coefficient of performance (COP). COP is defined as the ratio of the useful effects to the energy input. The useful effects include freshwater production and the cooling effect. The water consumption for evaporative cooling is expected to be supplied by the distillate produced in the HDH cycle, and the water production is calculated as

$$\dot{D}_{sys} = \dot{D}_{HDH} - \dot{D}_{IEC} = \dot{m}_{da}(\omega_4 - \omega_5) - \dot{m}_{da}(\omega_3 - \omega_2) \quad (11)$$

where $\dot{D}_{HDH}$ is the freshwater production of the HDH cycle, while $\dot{D}_{IEC}$ is the water consumption of the IEC unit.

The cooling capacity of the IEC unit is expressed as

$$\dot{Q}_{cool} = \dot{m}_{da}(h_{a1} - h_{a2}) \quad (12)$$

And the heat input to the HDH cycle is

$$\dot{Q}_{heat} = \dot{m}_h(h_{w11} - h_{w12}) \quad (13)$$

Finally, the overall COP is derived as [24]

$$COP = \frac{\dot{D}_{sys}h_{fg} + \dot{Q}_{cool}}{\dot{Q}_{heat} + W} \quad (14)$$

Here $W$ represents the power consumption in the IEC unit, including the fan and the sprayer pump. Electricity consumption of the HDH cycle is not considered because it is insignificant when compared to the heat input.

In addition to the COP, the exergy efficiency is also a powerful measurement of system efficiency. The exergy efficiency of a thermal system can be expressed as

$$\eta_{ex} = \frac{\dot{E}_{x,out}}{\dot{E}_{x,in}} \tag{15}$$

where $\dot{E}_{x,in}$ and $\dot{E}_{x,out}$ represent overall exergy input and output, respectively. For the integrated IEC-HDH cycle, the exergy output is derived as

$$\dot{E}_{x,out} = \dot{Q}_{cool}\left(1 - \frac{T_{a2}}{T_{a1}}\right) + \dot{D}_{sys} w_{sep} \tag{16}$$

The least work of separation for desalination, $w_{sep}$, is defined as the difference of Gibbs free energy between inlet and outlet streams [30]

$$w_{sep} = g_d + \left(\frac{1}{r} - 1\right) g_b - \frac{1}{r} g_f \tag{17}$$

In the above equation, $g$ represents the Gibbs free energy, and $r$ is the recovery ratio of the desalination system. Subscripts $d$, $b$, and $f$ represent the distillate, brine, and feed seawater. The detailed derivation is presented in [30].

Exergy input of the system is calculated as

$$\dot{E}_{x,in} = W + \dot{Q}_{heat}\left(1 - \frac{T_{a1}}{T_{w11}}\right) \tag{18}$$

## 5. Results and discussion

This section presents the performance of the IEC unit, the HDH cycle, and the integrated IEC-HDH cycle. Firstly the IEC is experimentally evaluated. Then the HDH cycle is analyzed using the experimental results of IEC as the input. Finally, the performance of the integrated system is derived.

### 5.1 Experimental results of IEC unit

Figure 4 portrays a typical temperature profile for the IEC unit. During the test, outdoor air was firstly heated using an external air heater. Once the desired outdoor temperature was obtained (at around 920 s), the spray pump was operated to supply water to the wet channels, and the temperatures of supply air and purge air started to drop due to the evaporative cooling effect. After another 1000 s the temperatures were stabilized and the system reaches steady-state. The unfluctuating results demonstrate excellent data reproductivity.

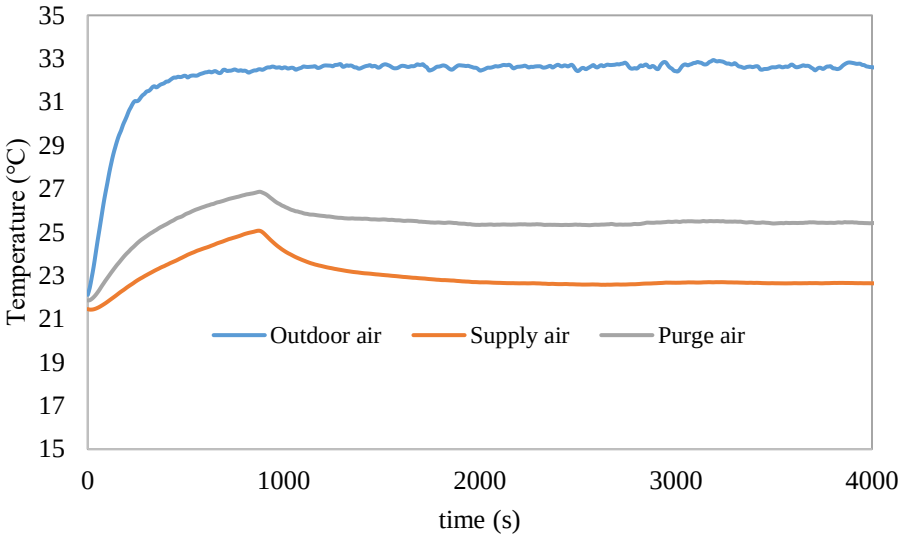


Figure 4 Transient temperature profile for outdoor air, supply air, and purge air

Figure 5 shows temperatures of supply air and purge air under different outdoor air temperatures. The humidity ratio of the intake air was fixed at 10.8 g/kg to meet the demand of thermal comfort, and the mass flowrate of the purge air was controlled to be equal to the supply air. Each data point is based on the average value of more than 20-min measurement after the system reached the steady-state. It is obvious from the figure that the IEC is able to reduce the supply air temperature by 6-17 ℃ depending on the outdoor condition. The higher the outdoor temperature, the more pronounced the temperature drop is. Under the range of outdoor air temperatures considered, the supply air is always below 25 ℃, demonstrating the good capability for the IEC unit to achieve thermal comfort in tropical areas.

The purge air temperature is also significantly reduced as compared to the intake air. Moreover, it is moisture content gets higher with RH >80% when leaving the wet channels. Such a cold and wet air stream is expected to promote humidifier performance when employed as the working air in the HDH cycle, which will lead to higher productivity and energy efficiency.

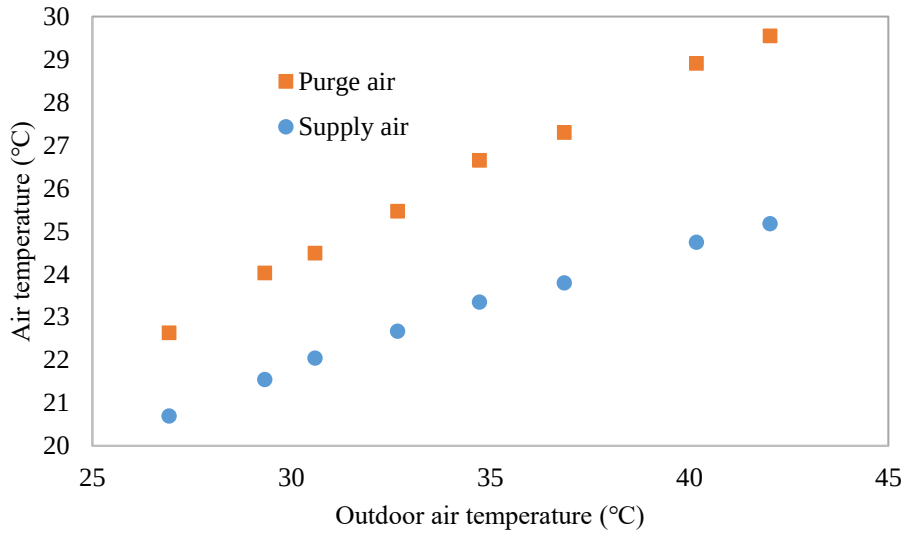

Figure 5 Temperatures for supply air and purge air under different ambient conditions

It should be noted that the above-mentioned results are based on a low outdoor air humidity of 10.8 g/kg. If the outdoor air humidity is higher, a dehumidifier is required to remove the moisture in order to meet the demand for thermal comfort and sustain the performance of the IEC unit.

## 5.2 Analytical results of the HDH cycle

After testing the IEC unit, this sub-section evaluates and compares different HDH cycles to highlight the advantages of the integrated IEC-HDH cycle. Three cycles are considered, namely, (1) the integrated IEC-HDH cycle, which uses the IEC purge air as the working air for HDH, (2) a basic HDH cycle that directly uses the outdoor air, and (3) a water-heated close-air-open-water (CAOW) cycle.

The developed model is firstly validated with data published in the literature [9, 31], and the results are provided in ***Appendix 1***. The air/water temperatures and the energy efficiencies calculated from the developed model agree well with literature data, demonstrating excellent prediction capability of the model.

Employing the validated model, the performances of different HDH cycles are compared. Figure 6 shows the productivity and GOR of three cycles under different mass flowrate ratios between water and air. The heat source temperature is 80 ℃ and the ambient temperature is 40 ℃. As described previously, the basic HDH cycle uses ambient air as the working media, while the IEC-HDH cycle employs the purge air (28.9 ℃, 85% RH). The flowrate of the dry air is kept fixed at 0.15 kg/s, which is equal to the IEC purge air flowrate. It is clearly seen from the figure that there is an optimal mass flowrate ratio that maximizes both the productivity and the GOR. The same observation has been reported in several previous studies [31-34]. A smaller feed flowrate results in insufficient humidification of the air, while a larger value leads to additional energy consumption to heat excessive seawater. Under the optimal feed flowrate, the integrated IEC-HDH cycle outperforms the other two in terms of both productivity and GOR. Productivity is improved by 15-20 L/hr, and the GOR is 70% higher.

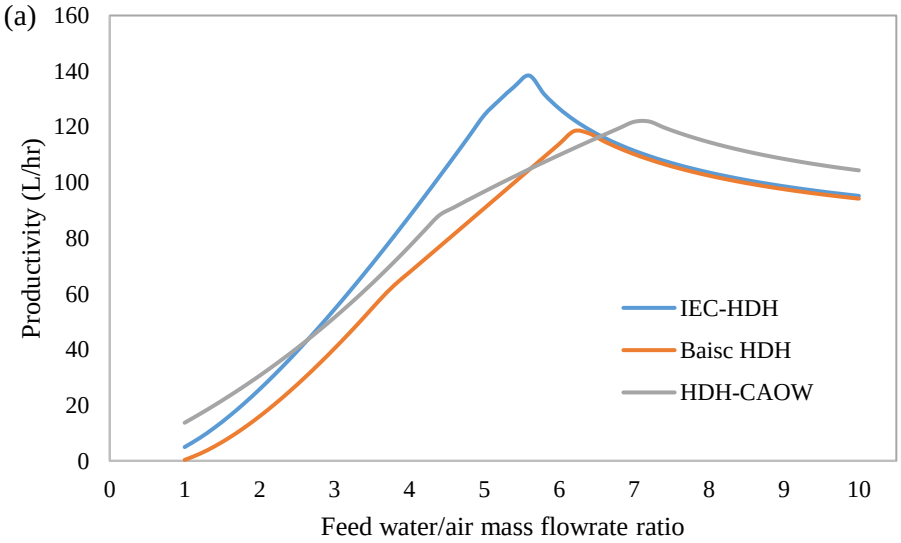

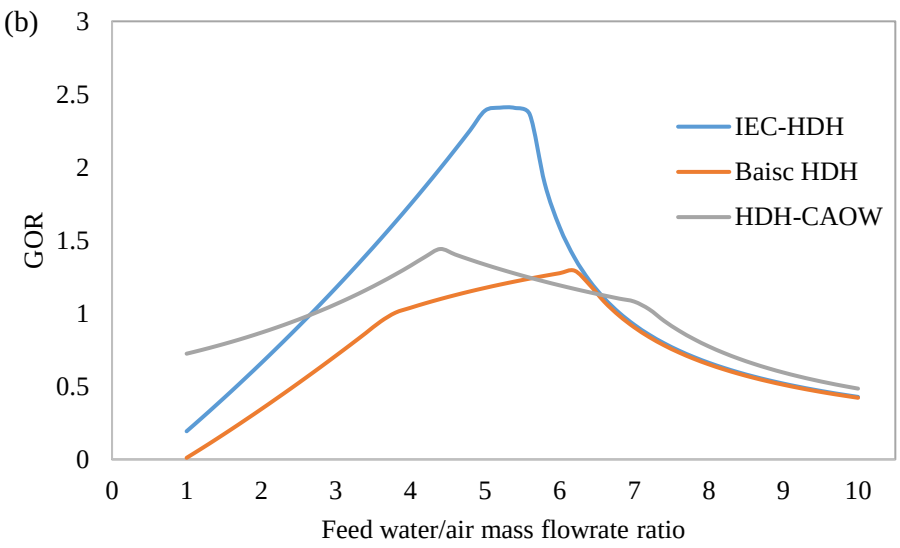


Figure 6 (a) Productivity and (b) GOR of different cycles under different mass flowrate ratios with air flowrate 0.15 kg/s, heat source temperature 80 ℃ and ambient temperature 40 ℃

Table 3 provides the states (temperature, enthalpy, and humidity ratio) of air and seawater at different locations for three HDH cycles. The locations of the points are indicated in Figure 1 and Figure 2. As can be seen from the table, the integrated IEC-HDH cycle is able to promote seawater evaporation due to a larger driving force, as indicated by a higher temperature and humidity ratio of the air leaving the humidifier (point 4). Moreover, the hot air is able to preheat the feed seawater to a higher temperature (point 7), thus reducing the heat input requirement. Consequently, the IEC-HDH cycle has better productivity and GOR than the other two cycles.

Table 3 Comparison of stream data for different cycles

| Point | Fluid | IEC-HDH | | | Basic HDH | | | HDH-CAOW | | |
|---|---|---|---|---|---|---|---|---|---|---|
| | | T (℃) | ω (g/kg) | h (kJ/kg) | T (℃) | ω (g/kg) | h (kJ/kg) | T (℃) | ω (g/kg) | h (kJ/kg) |
| 1 | Air | 40.0 | 10.8 | 68.05 | 40.0 | 10.8 | 68.05 | - | - | - |
| 2 | Air | 24.7 | 10.8 | 52.55 | 40.0 | 10.8 | 68.05 | - | - | - |
| 3 | Air | 28.9 | 21.4 | 83.55 | 40.0 | 10.8 | 68.05 | 49.3 | 84.7 | 269.03 |
| 4 | Air | 72.6 | 336.9 | 959.12 | 70.5 | 293.3 | 841.26 | 66.7 | 231.4 | 673.46 |
| 5 | Air | 55.5 | 120.4 | 369.06 | 51.6 | 96.5 | 302.16 | 49.3 | 84.7 | 269.03 |
| 6 | Water | 40.0 | - | 159.74 | 40.0 | - | 159.74 | 40.0 | - | 159.74 |
| 7 | Water | 66.1 | - | 264.55 | 60.1 | - | 242.03 | 61.3 | - | 245.04 |
| 8 | Water | 75.8 | - | 303.60 | 74.0 | - | 296.39 | 74.4 | - | 297.88 |
| 9 | Water | 39.5 | - | 157.73 | 46.8 | - | 187.00 | 54.3 | - | 217.19 |

Figure 7 shows the sensitivity of the GOR of the HDH cycle as a function of the purge air properties, i.e. velocity, relative humidity, and temperature. Since the maximum measurement uncertainty of these properties is 5%, as previously given in Table 1, these parameters are subjected to a variation of ±5% in the analysis. As can be seen from the figure, under the whole range of measurement uncertainties considered, the change of GOR is negligible. In other words, measurement uncertainties of the purge air properties have

marginal impacts on the analytical results of the HDH cycle, and the accuracy of the simulations can be guaranteed.

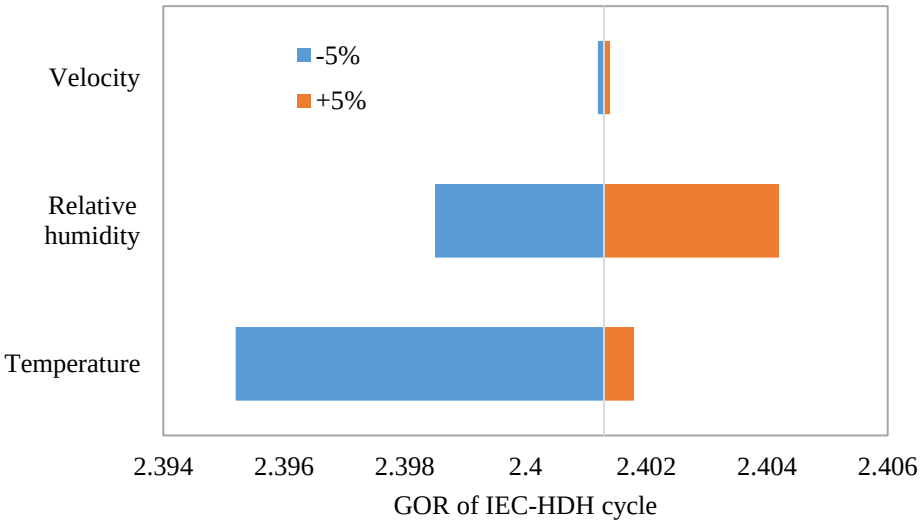


Figure 7 Sensitivity analysis of the GOR for the IEC-HDH cycle as a function of the purge air properties

Figure 8 compares the three cycles under different heat source temperatures under an ambient temperature of 40 ℃. Optimal seawater flowrates are adopted for each data point, and the values are provided in ***Appendix 2***. As expected, a higher heat source temperature provides a larger driving force for seawater evaporation, leading to higher freshwater yield, as shown in

Figure *8*(a). The energy consumption will also increase under a higher heat source temperature due to the need to heat air and seawater to higher temperatures. For the basic HDH cycle and the integrated IEC-HDH cycle, the benefit of higher productivity supersedes the negative effect of more energy consumption, and GOR is promoted at higher heat source temperatures, as can be seen in

Figure *8*(b). However, productivity improvement is less pronounced in the CAOW cycle, and the effect of more energy consumption is dominating. Therefore, the GOR of the CAOW cycle is lower under higher heat source temperatures. Under the temperature range considered, the IEC-HDH cycle has the highest GOR among the three cycles, and the improvement is more obvious when the heat source temperature is higher.

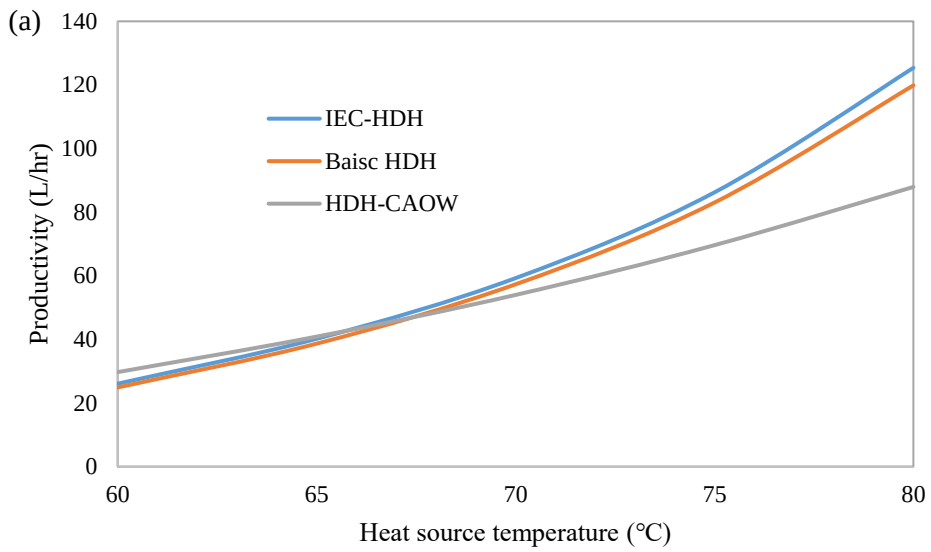


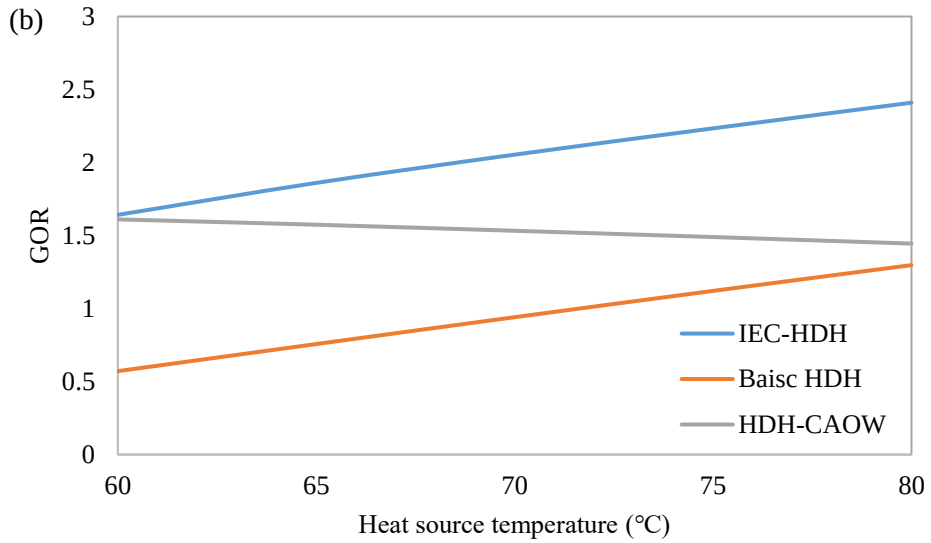


Figure 8 (a) Productivity and (b) GOR of different cycles under different heat source temperatures with air flowrate 0.15 kg/s, ambient temperature 40 ℃ and optimized feed flowrate

Figure 9 compares the three cycles under different ambient temperatures. Again, the seawater flowrate is optimized for each data point. The ambient temperature determines the feed seawater temperatures for all three cycles and the inlet air temperature for the basic HDH cycle, while the purge air temperatures shown in Figure 5 are employed for the IEC-HDH cycle. A higher ambient temperature is expected to have two conflicting effects. Firstly, it reduces productivity due to less effective condensation in the dehumidifier. Secondly, the heat consumption is reduced because of a smaller overall temperature gradient. The former effect is dominating in the basic HDH cycle and the IEC-HDH cycle, while the latter is more pronounced in the CAOW cycle. Therefore, GOR of the basic cycle and the IEC-HDH cycle decreases with increasing ambient temperature, while that of the CAOW cycle is increased. Despite different trends, the performance of the IEC-HDH cycle is better than the other two cycles over the whole range of ambient temperatures.

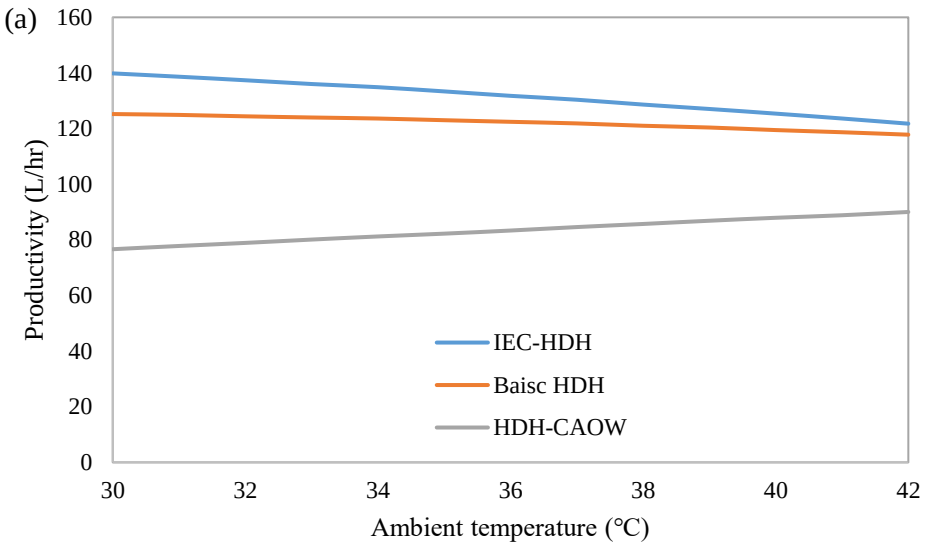


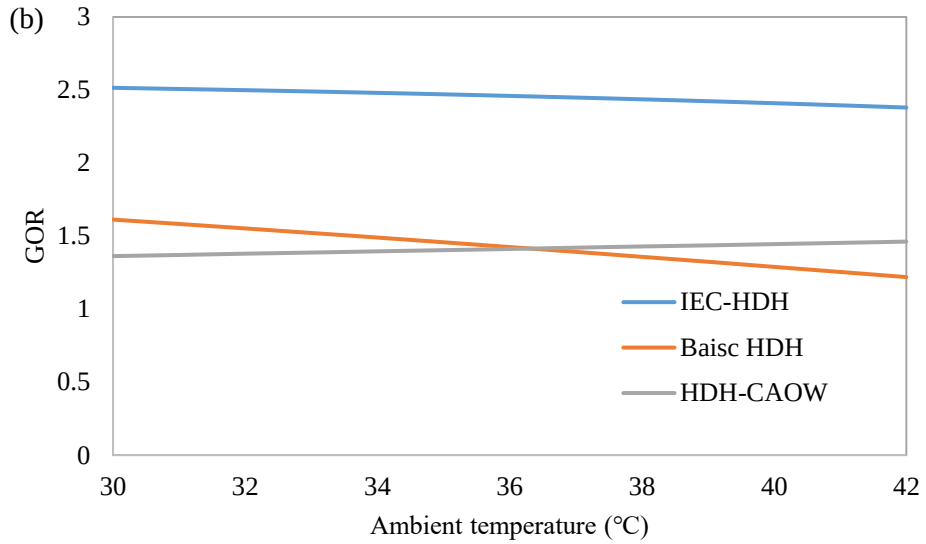


Figure 9 (a) Productivity and (b) GOR of different cycles under different ambient temperatures with air flowrate 0.15 kg/s, heat source temperature 80 ℃ and optimized feed flowrate

### 5.3 Performance of the integrated IEC-HDH cycle

From the above results, it can be concluded that the HDH cycle has better performance when employing purge air from IEC as the working medium, thus making the integrated IEC-HDH cycle more competitive than standalone IEC and HDH systems. To further demonstrate the benefits of system integration, this sub-section evaluates the overall energy efficiency of the combined IEC-HDH cycle and compares it with other similar systems.

When all the purge air is supplied to the HDH cycle, the capacity of HDH is much higher than IEC. Under the operating conditions considered, heat input to HDH is 24-30 kW, while electricity consumption of IEC is marginal at 120 W. Meanwhile, the cooling capacity of IEC ranges 1-2.5 kW, while the equivalent latent

heat of vaporization in HDH is 90-100 kW. Also, the water consumption of IEC accounts for only 3-6% of HDH productivity. Therefore, the overall COP is dominated by the HDH cycle. As shown by the blue line in Figure 10, the COP of the integrated cycle is almost the same as the GOR of the HDH cycle.

In practical applications, the amount of purge air being supplied to the HDH cycle can be regulated according to the actual needs of cooling load and freshwater. In this case, the COP will suffer from a minor drop, because water consumption of IEC will become more significant when HDH productivity is lower. The COP under different purge air supply ratios is also plotted in Figure 10, which decreases slightly when less purge air is supplied to HDH.

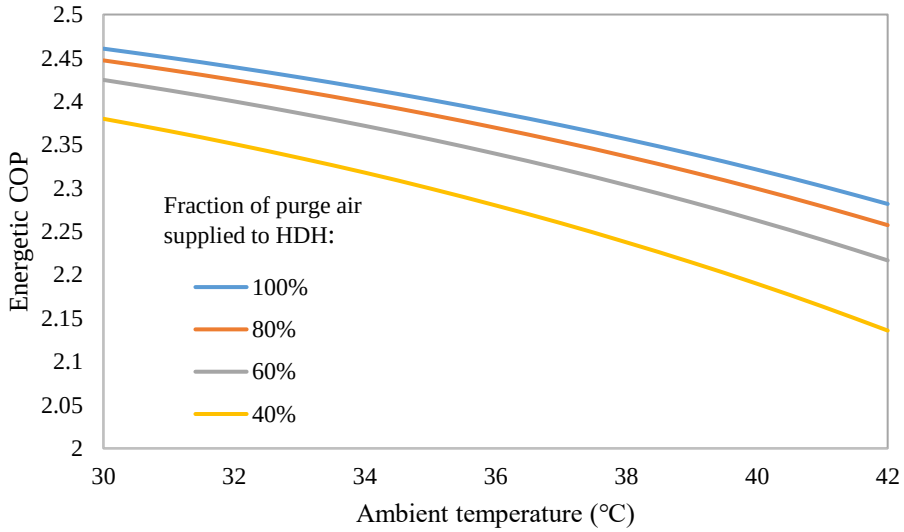


Figure 10 Energetic COP for the integrated IEC-HDH cycle

Figure 11 shows the exergy efficiency of the system under different ambient and heat source temperatures. For a given heat source temperature, the exergy efficiency of the combined cycle increases at higher ambient temperatures. This is because the overall temperature difference in the system becomes smaller when the ambient temperature is higher. Consequently, irreversible dissipations during heat and mass transfer are reduced, leading to a higher exergy efficiency. The exergy efficiency is promoted by a lower heat source temperature, which is due to a reduced exergy input to the system.

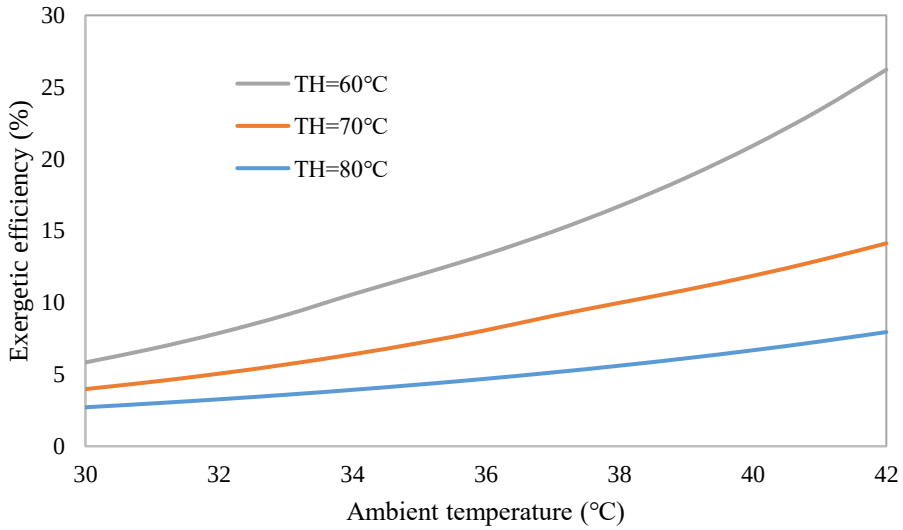


Figure 11 Exergy efficiency for the integrated IEC-HDH cycle

Figure 12 compares the COP of the proposed system with other systems that simultaneously produce cooling effects and freshwater, including an adsorption (AD) cooling/desalination system [23], an AD chiller integrated with HDH [7], an absorption (AB) chiller integrated with HDH [8], and a combined refrigeration (REF) and HDH system [10, 11]. As shown in the figure, the COP of the proposed IEC-HDH cycle outperforms the AD system and the AB-HDH cycle by several times due to optimized design and operation. The AD-HDH and REF-HDH systems have higher COP, but they have several limitations. For example, the adsorption beds require a vacuum condition, and the REF-HDH system consumes electricity. On the other hand, the proposed IEC-HDH cycle operates under the ambient condition and is driven by low-grade heat. Therefore, the proposed IEC-HDH represents a cost-effective and environmental-friendly solution for providing cooling and freshwater in remote regions. If a higher COP is desired, the IEC-HDH cycle can also be integrated with AD or REF systems to further increase its energy efficiency.

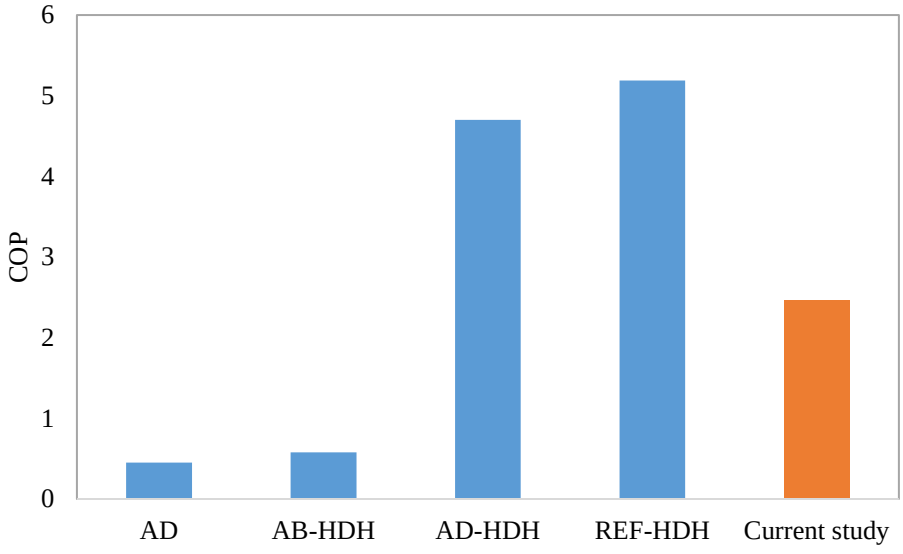


Figure 12 Comparison of COP for different cooling-freshwater cogeneration systems

## 6. Conclusions

In this study, a hybrid system integrating indirect evaporative cooler (IEC) and humidification-dehumidification desalination (HDH) has been evaluated. Experimental tests are firstly conducted for a pilot IEC unit to obtain the temperatures and humidity of the outlet air streams. Then the HDH cycle is theoretically analyzed employing the purge air from IEC as the working air. The overall energy efficiency of the hybrid IEC-HDH cycle is also evaluated and compared with other similar systems. The main findings are highlighted as follows:

(1) The designed IEC unit is able to cool down the outdoor air to below 25 ℃ without increasing the moisture content, and the purge air temperature is also 5-10 ℃ lower than the intake air temperature;
(2) Employing the IEC purge air as the working air, the HDH cycle has a GOR that ranges 1.6-2.4, which is higher than standalone HDH systems operating under the same conditions;
(3) Productivity and GOR of the HDH cycles are promoted under higher heat source temperatures and lower ambient temperatures, while there is an optimal value of the water/air mass flowrate ratio that maximizes the system performance;
(4) Overall COP of the combined IEC-HDH cycle is close to the GOR of the HDH system due to negligible energy consumption of the IEC cycle, and the COP decreases slightly when the capacity of the HDH cycle is smaller;
(5) The exergy efficiency of the combined IEC-HDH cycle spans 3-26%, and it is promoted by higher ambient temperatures and lower heat source temperatures;
(6) The COP of the proposed IEC-HDH system outperforms the adsorption cycle and the integrated absorption-HDH cycle, and its value can be further increased via hybridization with adsorption cycles or vapor compression refrigeration cycles.

## Nomenclature

| | |
|---|---|
| $C$ | Heat capacity, W/℃ |
| $COP$ | Coefficient of performance |
| $D$ | Freshwater productivity, kg/s |
| $E$ | Exergy, kW |
| $GOR$ | Gained-output ratio |
| $h$ | Specific enthalpy, kJ/kg |
| $m$ | Mass flowrate, kg/s |
| $Q$ | Heat flux, W |
| $r$ | Recovery ratio, % |
| $T$ | Temperature, ℃ |
| $W$ | Electricity consumption, W |

Greek letters

| | |
|---|---|
| $\varepsilon$ | Effectiveness |
| $\eta$ | Efficiency, % |
| $\omega$ | Humidity ratio, kg/kg |

Subscripts

| | |
|---|---|
| *a* | Air |
| *b* | Brine |
| *cool* | Cooling |
| *d* | Dehumidifier; distillate |
| *deh* | Dehumidifier |
| *ex* | Exergy |
| *f* | Feed seawater |
| *h* | Heater |
| *heat* | Heating |
| *hex* | Heat exchanger |
| *hum* | Humidifier |
| *ideal* | Ideal state |
| *in* | Input |
| *max* | Maximum |
| *min* | Minimum |
| *out* | Output |
| *sep* | Seperation |
| *sys* | System |
| *w* | Water |

**Acknowledgement**

This research was supported by the Water Desalination and Reuse Center (WDRC), King Abdullah University of Science and Technology (KAUST).

## Appendix 1 Model validation

The simulation results of the proposed model is compared with data acquired from the literature. Table A1 compares the temperatures of air/water at different locations with the results presented by Sadeghi et al. [9]. RH of the moist air is assumed to be 90% at the outlets of the humidifier and the dehumidifier, while humidifier/dehumidifier effectiveness is 0.85, and water/air mass flowrate ratio is 1.7. Feed temperature (point 6) and top water temperature (point 8) reported in [9] are employed as the model input to calculate the temperatures in the remaining locations. As shown in the figure, the predicted values adhere closely to those reported in the literature, and the maximum discrepancy is 1.8%.

Table A1 Comparison of air/water temperatures between the current study and literature

| Point | Sadeghi et al. [9] | Current work | Difference |
|---|---|---|---|
| 3 | 28.67 | 28.45 | 0.8% |
| 4 | 22.13 | 22.42 | 1.3% |
| 5 | 28.67 | 28.45 | 0.8% |
| 6 | 20 | 20 | 0.0% |
| 7 | 23.74 | 23.44 | 1.3% |
| 8 | 27.96 | 27.96 | 0.0% |
| 9 | 24.12 | 24.55 | 1.8% |

Figure A1 compares the predicted GOR with data reported by Narayan et al. [31]. The air is assumed to be saturated in both humidifier and dehumidifier, and effectiveness is 0.92. The predicted values agree well with the values reported in [31] under different mass flowrate ratios and top temperatures, and the maximum discrepancy is 4%.

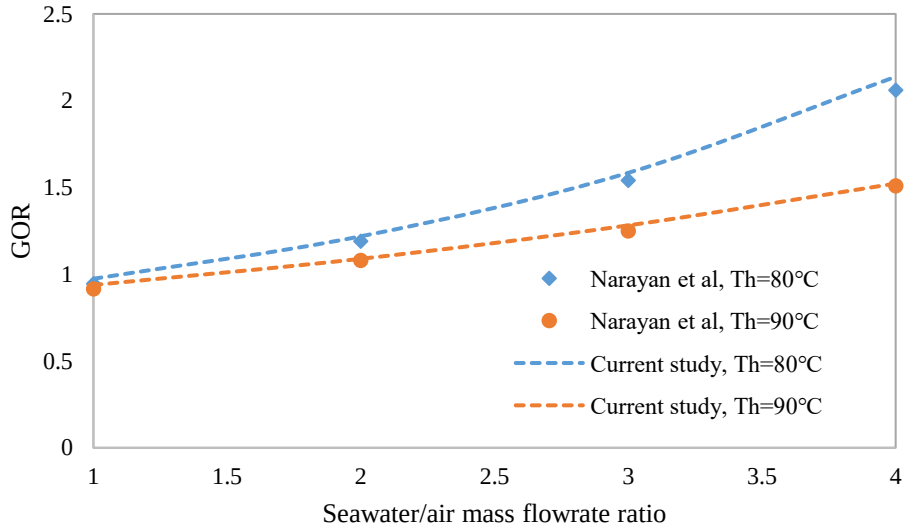


Figure A1 Comparison of gain-output ratio between current study and literature

## Appendix 2 Optimal water/air mass flowrate ratio

The optimal feed water/air mass flowrate ratio varies with the operating conditions. Its value increases with the increase of heat source temperature and ambient temperature, as shown in Figure A2.The same trend has also been reported in the literature for a CAOW cycle [32]. The required feed flowrate for the proposed IEC-HDH cycle is lower than the basic IEC cycle. Its value is also lower than the CAOW cycle when the heat source temperature is below 75 ℃.

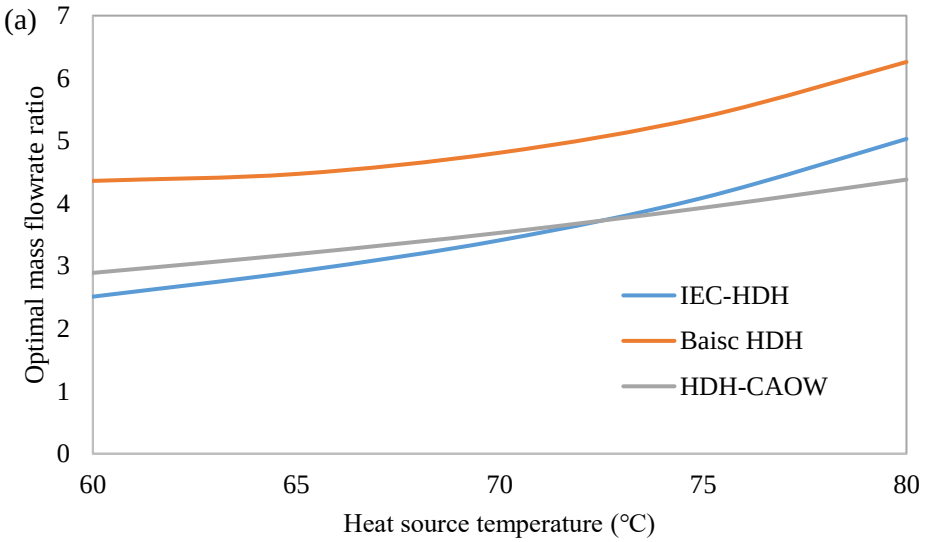

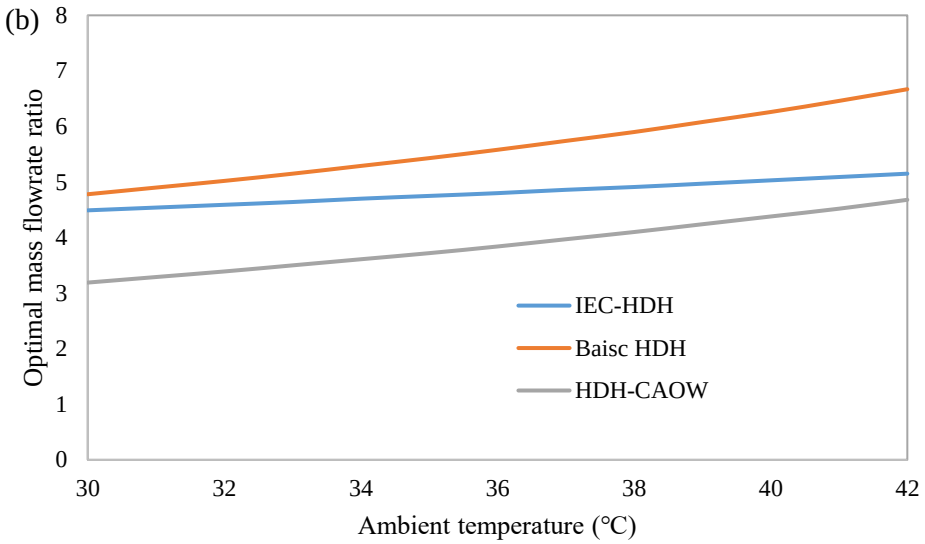


Figure A2 Optimal feed water/air mass flowrate ratio for (a) different heat source temperatures and ambient temperature of 40 ℃ and (b) different ambient temperatures under heat source temperature of 80 ℃

## References


1. Parmigiani, L., *Water and energy in the GCC: securing scarce water in oil-rich countries.* 2015.
2. Eveloy, V. and D.S. Ayou, *Sustainable district cooling systems: Status, challenges, and future opportunities, with emphasis on cooling-dominated regions.* Energies, 2019. **12**(2): p. 235.
3. Jones, E., M. Qadir, M.T. van Vliet, V. Smakhtin, and S.-m. Kang, *The state of desalination and brine production: A global outlook.* Science of the Total Environment, 2019. **657**: p. 1343-1356.
4. Fath, H., A. Sadik, and T. Mezher, *Present and future trend in the production and energy consumption of desalinated water in GCC countries.* Int. J. Therm. Environ. Eng, 2013. **5**(2): p. 155-165.
5. Narayan, G.P. and J.H. Lienhard, *Humidification dehumidification desalination.* Desalination: Water from Water, 2014: p. 425-472.
6. Mahmood, M.H., M. Sultan, T. Miyazaki, S. Koyama, and V.S. Maisotsenko, *Overview of the Maisotsenko cycle–A way towards dew point evaporative cooling.* Renewable and sustainable energy reviews, 2016. **66**: p. 537-555.
7. Qasem, N.A. and S.M. Zubair, *Performance evaluation of a novel hybrid humidification-dehumidification (air-heated) system with an adsorption desalination system.* Desalination, 2019. **461**: p. 37-54.
8. Chiranjeevi, C. and T. Srinivas, *Combined two stage desalination and cooling plant.* Desalination, 2014. **345**: p. 56-63.
9. Sadeghi, M., M. Yari, S. Mahmoudi, and M. Jafari, *Thermodynamic analysis and optimization of a novel combined power and ejector refrigeration cycle–Desalination system.* Applied energy, 2017. **208**: p. 239-251.
10. He, W., D. Han, and C. Ji, *Investigation on humidification dehumidification desalination system coupled with heat pump.* Desalination, 2018. **436**: p. 152-160.

11. He, W., T. Wen, D. Han, L. Luo, R. Li, and W. Zhong, *Energetic, entropic and economic analysis of a heat pump coupled humidification dehumidification desalination system using a packed bed dehumidifier.* Energy Conversion and Management, 2019. **194**: p. 11-21.
12. Xu, H., X. Sun, and Y. Dai, *Thermodynamic study on an enhanced humidification-dehumidification solar desalination system with weakly compressed air and internal heat recovery.* Energy conversion and management, 2019. **181**: p. 68-79.
13. Sohani, A., H. Sayyaadi, and S. Hoseinpoori, *Modeling and multi-objective optimization of an M-cycle cross-flow indirect evaporative cooler using the GMDH type neural network.* International Journal of Refrigeration, 2016. **69**: p. 186-204.
14. Sohani, A., H. Sayyaadi, and M. Zeraatpisheh, *Optimization strategy by a general approach to enhance improving potential of dew-point evaporative coolers.* Energy Conversion and Management, 2019. **188**: p. 177-213.
15. Akhlaghi, Y.G., A. Badiei, X. Zhao, K. Aslansefat, X. Xiao, S. Shittu, and X. Ma, *A constraint multi-objective evolutionary optimization of a state-of-the-art dew point cooler using digital twins.* Energy Conversion and Management, 2020. **211**: p. 112772.
16. Cui, X., M. Islam, B. Mohan, and K. Chua, *Theoretical analysis of a liquid desiccant based indirect evaporative cooling system.* Energy, 2016. **95**: p. 303-312.
17. Woods, J. and E. Kozubal, *A desiccant-enhanced evaporative air conditioner: Numerical model and experiments.* Energy Conversion and Management, 2013. **65**: p. 208-220.
18. Pandelidis, D., S. Anisimov, W.M. Worek, and P. Drąg, *Comparison of desiccant air conditioning systems with different indirect evaporative air coolers.* Energy conversion and management, 2016. **117**: p. 375-392.
19. Cui, X., K. Chua, M. Islam, and K. Ng, *Performance evaluation of an indirect pre-cooling evaporative heat exchanger operating in hot and humid climate.* Energy Conversion and Management, 2015. **102**: p. 140-150.
20. Cui, X., K. Chua, and W. Yang, *Use of indirect evaporative cooling as pre-cooling unit in humid tropical climate: an energy saving technique.* Energy Procedia, 2014. **61**: p. 176-179.
21. Tariq, R., N.A. Sheikh, J. Xamán, and A. Bassam, *An innovative air saturator for humidification-dehumidification desalination application.* Applied energy, 2018. **228**: p. 789-807.
22. Saghafifar, M. and M. Gadalla, *Analysis of Maisotsenko open gas turbine power cycle with a detailed air saturator model.* Applied Energy, 2015. **149**: p. 338-353.
23. Wang, X. and K.C. Ng, *Experimental investigation of an adsorption desalination plant using low-temperature waste heat.* Applied Thermal Engineering, 2005. **25**(17-18): p. 2780-2789.
24. Kabeel, A. and M. Abdelgaied, *Hybrid system of an indirect evaporative air cooler and HDH desalination system assisted by solar energy for remote areas.* Desalination, 2018. **439**: p. 162-167.
25. OMIGA, *Transition Joint-Style Thermistor Probes For Immersion Applications.* Retrived from https://br.omega.com/omegaFiles/temperature/pdf/TJ36-44004.pdf, June 2020.
26. Inc., D.C., *FH-Series.* Retrived from https://degreec.com/products/fh400, June 2020.
27. Narayan, G.P., R.K. McGovern, and S.M. Zubair, *High-temperature-steam-driven, varied-pressure, humidification-dehumidification system coupled with reverse osmosis for energy-efficient seawater desalination.* Energy, 2012. **37**(1): p. 482-493.
28. Sharqawy, M.H., J.H. Lienhard, and S.M. Zubair, *Thermophysical properties of seawater: a review of existing correlations and data.* Desalination and water treatment, 2010. **16**(1-3): p. 354-380.
29. Herrmann, S., H.-J. Kretzschmar, and D.P. Gatley, *Thermodynamic properties of real moist air, dry air, steam, water, and ice (RP-1485).* HVAC&R Research, 2009. **15**(5): p. 961-986.
30. Chen, Q., M.K. Ja, Y. Li, and K. Chua, *On the second law analysis of a multi-stage spray-assisted low-temperature desalination system.* Energy conversion and management, 2017. **148**: p. 1306-1316.

31. Narayan, G.P., M.H. Sharqawy, J.H. Lienhard V, and S.M. Zubair, *Thermodynamic analysis of humidification dehumidification desalination cycles.* Desalination and water treatment, 2010. **16**(1-3): p. 339-353.
32. Sharqawy, M.H., M.A. Antar, S.M. Zubair, and A.M. Elbashir, *Optimum thermal design of humidification dehumidification desalination systems.* Desalination, 2014. **349**: p. 10-21.
33. Hermosillo, J.-J., C.A. Arancibia-Bulnes, and C.A. Estrada, *Water desalination by air humidification: Mathematical model and experimental study.* Solar Energy, 2012. **86**(4): p. 1070-1076.
34. Yuan, G., Z. Wang, H. Li, and X. Li, *Experimental study of a solar desalination system based on humidification–dehumidification process.* Desalination, 2011. **277**(1-3): p. 92-98.